Hindawi
Journal of Spectroscopy
Volume 2022, Article ID 1874173, 7 pages
https://doi.org/10.1155/2022/1874173

Research Article

Evaluation of a Peak-Free Chemometric Laser-Induced Breakdown Spectroscopy Method for Direct Rapid Cancer Detection via Trace Metal Biomarkers in Tissue

Otieno Emily Akinyi, Angeyo Hudson Kalambuka, and Alix Dehayem-Kamadjeu

Department of Physics, University of Nairobi, P.O. Box 30197-00100, Nairobi, Kenya

Correspondence should be addressed to Angeyo Hudson Kalambuka; hkalambuka@uonbi.ac.ke

Received 19 March 2022; Accepted 15 September 2022; Published 26 October 2022

Academic Editor: Davidson Sajan

The ability to perform direct rapid analysis in air and at atmospheric pressure is a remarkable attraction of laser-induced breakdown spectroscopy (LIBS) for the diagnostic quantification of disease biomarker metals in body tissue. However, accurate trace analysis is limited by matrix effects and a pronounced background that masks the subtle (peak-free) analyte signals because tissue plasma is dense and most lines are optically thick. In this work, a peak-free chemometric LIBS method based on a single-shot (for rapidity and nondestructiveness) and an artificial neural network multivariate calibration strategy with spectral feature selection was evaluated for its utility for direct trace quantitative analysis of copper (Cu), iron (Fe), manganese (Mg), magnesium (Mg), and zinc (Zn) in model soft body tissue. The spectral signatures corresponding to the biometals (so-called because the metals are intrinsic to tissue biochemistry) were generated by spiking their known human-body-representative concentrations in molten paraffin wax. The developed multivariate analytical model achieved ≥95% accuracy as determined from the analysis of oyster tissue-certified reference material. The analytical models were tested on the liver, breast, and abdominal tissue biopsies. The results of applying the model to the clinical tissues indicated the absence or presence (including severity) of cancer as either malignant or benign, in agreement with the pathological examination report.

1. Introduction

In laser-induced breakdown spectroscopy (LIBS), the microplasma that is formed when the laser ablates a sample is a "spectral fingerprint" of the sample matrix. Therefore, LIBS has great potential in medicine, where it may be used to gain diagnostic information by analysing anatomical specimens such as body fluids and tissue. The trace biometals thereby detected may be explored and used as disease biomarkers because they are crucial for biopathological processes (a quarter to a third of all proteins require them to carry out their functions).

A promising application is the elusive early cancer diagnosis which may be realized by providing noninvasive detection and identification of specific trace metal biomarkers in tissue because the tedious and destructive sample preparations required by other methods are in the LIBS technique inapplicable. Unfortunately, LIBS spectra in air and atmospheric pressure are adversely affected by matrix effects, shot-to-shot fluctuations, and self-absorption [1–3]. Furthermore, LIBS signals suffer from intensity and reproducibility degradation due to the softness, moisture content, and heterogeneity of tissue samples [4, 5]. Biological tissues contain trace biometals in very low concentrations [6]. Therefore, LIBS spectra of trace biometals from soft tissue show only a small number of subtle spectral lines from the biometals amid pronounced background and noise.

The technical, theoretical, and mathematical aspects of LIBS are well reported [7–11]. It remains to understand more about the dynamics of how laser light interacts with tissue materials in order to fully realize the utility of LIBS for disease diagnostics. LIBS analysis of trace metals in tissues

has been reported in the past, but the concentration levels of the metals of interest were either near or below the detection limit (DL). The well-known limitation of LIBS, namely, the relatively high DL of some metals with respect to their physiological levels has been pointed out by Santos Jr. et al. [12]. However, Adamson and Rehse [13] demonstrated DL <1 ppm for trace aluminium (Al) embedded as nanoparticles in surrogate tissue using LIBS. To achieve this, the authors used a calibration curve normalized by the nearby calcium (Ca) II line at 393.366 nm. Most quantitative LIBS methods involve univariate calibration curve and/or calibration-free approaches [14]. In univariate analysis, the useful spectral lines are carefully selected according to prior knowledge of the elemental components and biochemical characteristics of specific tissues, a laborious procedure. Needless to reiterate that the analytical approaches often fail to obtain the desired results for complex matrix samples. Furthermore, it is difficult to get suitable matrix-matched standards, making LIBS at best a semiquantitative tool for trace metal analysis in biological matrices. The challenge is how to improve the accuracy and speed of trace analysis by extracting useful analytical information from the LIBS high dimensionality data. Human tissues are molecularly complex and therefore nonlinear. Therefore, more robust approaches are needed for evaluation of the physiological levels of trace biometals by extracting characteristic spectral information while suppressing the spectral interference and noise.

Multivariate chemometrics analysis methods [15–17] are applicable in this respect because the LIBS spectral signal consists of a series of vector data with interdependent variables. Chemometrics methods take into account nearly all the variables in the spectra, remove unnecessary and correlated information, and extract the most relevant variables. The errors generated by random and various nontarget factors in the spectra are also reduced. Among the available methods of regression analysis in chemometrics, artificial neural networks (ANNs) are the most "intelligent" enough to learn, memorize, and create relationships among spectral data without the need for characteristic spectral information [18].

The feasibility of using low signal-to-noise ratio (SNR) analyte profiles (here called peak-free) in LIBS was demonstrated when arsenic (As), chromium (Cr), copper (Cu), lead (Pb), and titanium (Ti) were modelled for direct trace (quantitative) analysis using partial least squares (PLS) and artificial neural networks (ANNs) [19], where ANNs were noted to be more robust than PLS at modelling spectral nonlinearity and correcting matrix effects. In the biomedical applications of LIBS, a single biomarker approach is highly unlikely to yield results that have diagnostic accuracy; therefore, the idea of using a *basket* of biomarkers has been suggested [20, 21]. In this work, a chemometric peak-free LIBS approach was evaluated for its utility for direct, rapid but accurate trace quantitative analysis of copper (Cu), iron (Fe), manganese (Mn), magnesium (Mg), and zinc (Zn) simultaneously in soft body tissue. Such analysis would be useful in disease diagnostics applications based on absolute concentrations as well as the multivariate correlations and alterations of the analysed biometals (as the disease biomarkers) in body tissue as opposed to the practice of exploiting relative increases or decreases in intensities of major lines. The emphasis on rapid (single-shot) analysis and weak signals is crucial for clinical applications of LIBS.

2. Materials and Methods

2.1. Preparation of Model Tissue. Standard solutions of the target trace biometals were prepared by dissolving known amounts of analytical grade salts (copper nitrate ($Cu(NO_3)_2.3H_2O$), iron chloride ($FeCl_3.8H_2O$), ammonium iron (I) sulphate ($NH_4Fe(SO_4)_2.6H_2O$), zinc nitrate ($Zn(NO_3)_2.6H_2O$), magnesium chloride ($MgCl_2.6H_2O$), manganese chloride ($MnCl_2.4H_2O$), and potassium permanganate ($KMnO_4$)) in ethanol. The representative concentrations were selected in the ranges in which they occur in the human soft body tissues [22]: Fe: 30–170 μg/g, Mg: 962–502 μg/g, Zn: 20–200 μg/g, Cu: 1–10 μg/g, and Mn: 1–30 μg/g. The spiking concentration ranges were distributed using a research randomizer.

About 2 mL of molten paraffin wax was poured into a mould into which 5 mL of the prepared mixture was added. The mixture was then stirred to ensure homogeneity. Stirring was done while the mixture was being heated at 78°C to ensure that ethanol and acetone boiled off. The mould was covered with an embedding cassette and placed in a freezer to cool and form a block. The block was sliced to 2 cm thickness, each weighing ~2 g for LIBS analysis. Oyster tissue (NIST 1566B) powder was placed in a hydraulic press to also form method reference pellets of ~2 g each.

2.2. Preparation of Human Cancer Tissue Biopsy Samples. One (1) breast, two (2) liver, and one (1) abdominal tissue needle biopsies, which had been extracted through a routine surgical operation and histopathologically examined, were donated by Kenyatta National Referral Hospital. The tissues were trimmed to 2 mm thickness and placed in 10% formalin in labelled bottles. They were dehydrated by soaking in absolute alcohol three times successively for an hour each. The tissue samples were thereafter cleared of alcohol by soaking in 50 : 50 alcohol for an hour, followed by toluene in three stages lasting 30 minutes each. The tissues were dipped into a mould filled with molten paraffin wax, previously placed in an oven at 58°C, and brought back to the oven overnight for infiltration of wax to fill up the spaces left in the tissue. The following day, the tissues were embedded in fresh molten wax at 58°C in moulds and left to cool at room temperature. The blocks that formed were labelled and trimmed on the surface until the tissue was visible. They were finally processed and fixed in paraffin wax to make 2 cm thick blocks from which 3 μm thin sections were prepared on Mylar films for LIBS analysis.

2.3. LIBS Spectral Acquisition and Processing. The LIBS system that was used in this work is a pulsed ND: YAG laser with a maximum energy of 50 mJ operating at a fundamental wavelength of 1064 nm and a 9 ns pulse width. The laser is fired onto a sample, directed by a focusing lens (focal length

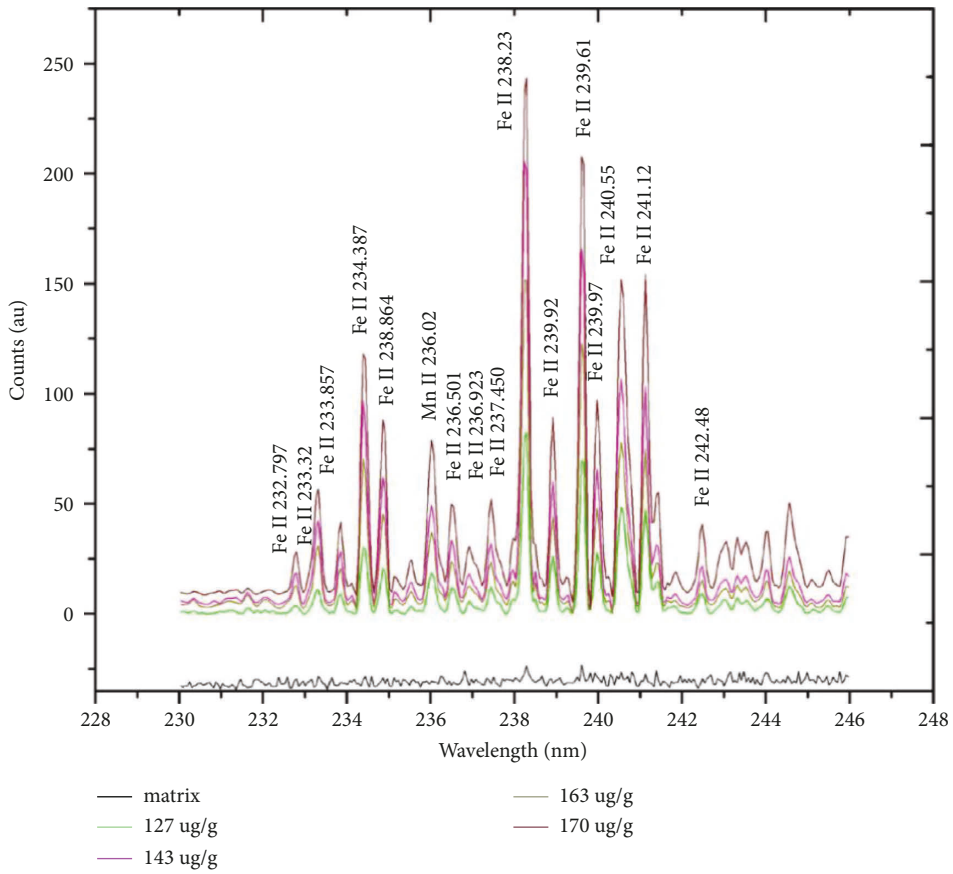

Figure 1: Laser-induced breakdown spectroscopy spectral overlay of model tissue samples with the blank matrix showing the difference in concentration levels or absence of iron in the base matrix.

of 10.16 cm), exciting it to produce a microplasma that is characteristic of the sample under analysis. The optical-to-sample distance was maintained at 30 mm following optimization. A fibre optical cable of 0.22 numerical aperture and 101 mm focal length collects the emission from the plasma plume through a lens into a set of seven HR 2000 atomic emission spectrometers in the spectral range of 200–980 nm, which spectrally disperse the radiation. Spectral data are acquired simultaneously and displayed on the computer screen with the help of OOILIBS software. Each charge coupled device (CCD) detector has 2048 pixels and an optical resolution of 0.065 nm.

Figure 1 shows examples of the LIBS spectral responses of Fe in typical soft body tissue as indicated by the detected lines whose intensity clearly steadily increases with the spiked concentration of Fe in the blank matrix. From this, it is easy to differentiate between self-absorbed lines and resonant lines, as well as those with good oscillator strength and those that are interference-free to be used as potential candidates for multivariate calibration using spectral feature selection. The detectability of Fe by LIBS is demonstrated in Figure 2 using a clinically acquired liver biopsy sample.

As LIBS spectral responses from biomatrix analytes suffer from matrix effects, the spectra require preprocessing [23] because the intensity of the emission lines observed is a

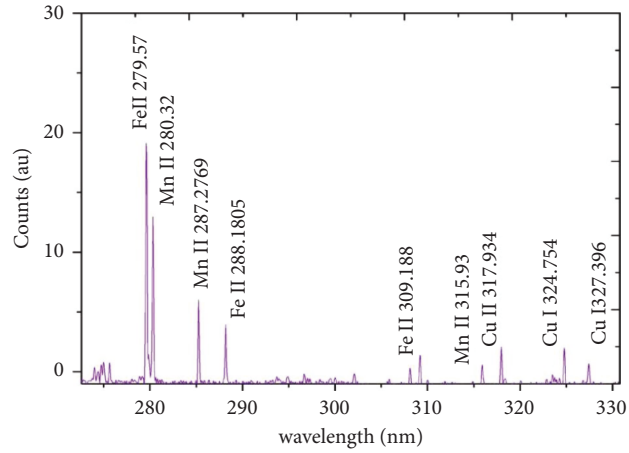

Figure 2: Example of a laser-induced breakdown spectroscopy spectrum of liver cancer tissue showing the lines of copper, manganese, and iron identified in the spectral region of 275–330 nm.

function of both the concentrations of the elements of interest as well as the thermochemical properties of the matrix that contains them. Preprocessing of spectra is essential to reduce noise and matrix effects. For this purpose, denoising, smoothing, baseline correction, and mean-cantering techniques were employed. Smoothing was done using the

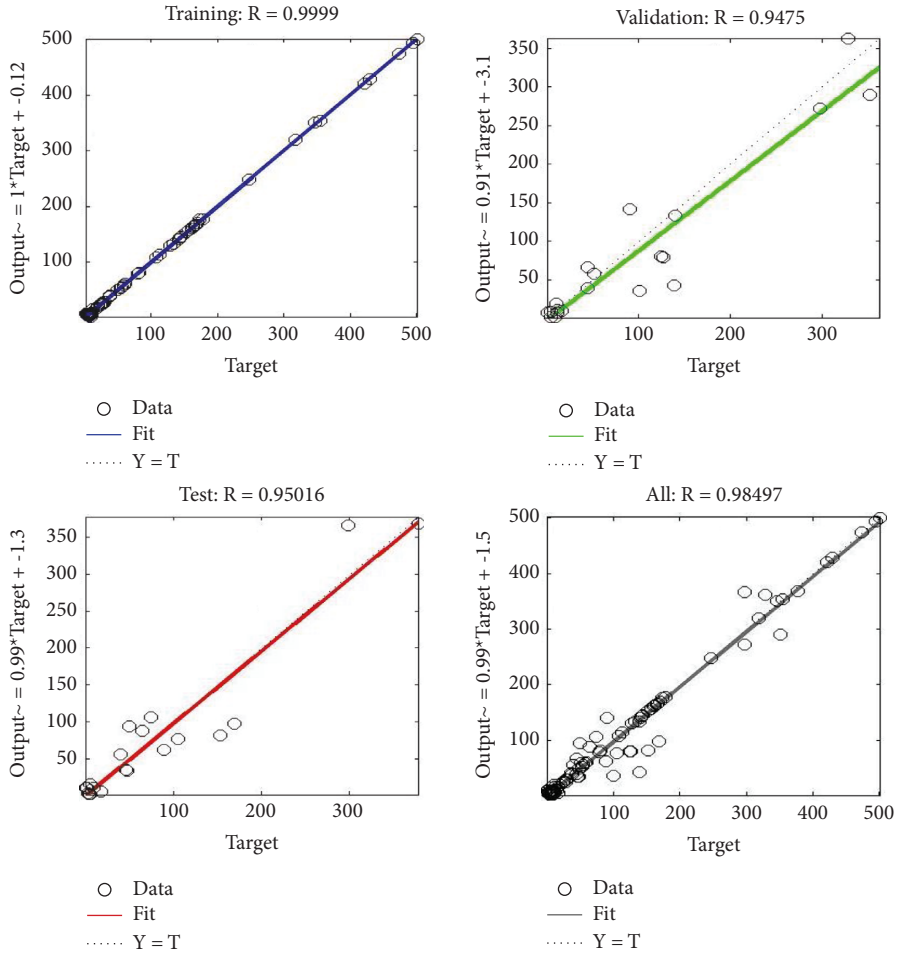

Figure 3: Regression curves of the artificial neural network model showing regression coefficient values for training curves.

Sivitzky Golay technique to obtain clear spectral line profiles, while wavelet transforms were used for denoising. Mean cantering enabled all the data across the spectral region to be involved in the modelling.

2.4. Multivariate Calibration for Quantitative Analysis. In this work, spectral features corresponding to Cu, Mn, Mg, Zn, and Fe of the model tissue samples were used to train the ANN model for trace quantitative analysis using MATLAB software. A recent review [24] sheds good light on ANN-based LIBS. ANN is one of the computational ways of mapping nonlinear input data to a target space. The most common of the network architectures is the multilayer feed-forward system, in which the input data proceed forward only (to the hidden layer and then to the output layer) and never make loops, as opposed to other techniques like the recurrent neural network system [25]. The power of the network depends on the transfer function, the learning rule, and the network architecture [26]. During training of the network, the neurons are optimized until the error in prediction is minimized and the network attains the desired level of accuracy. The trained network can then be given new input data to predict the output [27]. In this work, the best conditions were 3 neurons and a feed-forward back propagation algorithm. The model was trained using 60% of the data, 20% was used for validation, while the remaining 20% was used for testing. The model was trained a number of times until the one with the root mean square error of calibration (RMSEC) and regression coefficient (R^2) value closest to 1 was achieved. The model regression curves for training, validation, testing, and the overall curve are shown in Figure 3. The regression curves for Cu, Fe, Zn, Mn, and Mg, showing predicted concentration versus known concentration, are shown in Figures 4–8.

The NIST 1566B standard was used to estimate the analytical accuracy of the developed calibration model. In Table 1, the predicted values are compared against the standard reference values. It is noted that the ANN model is suitable for the determination of the concentration of Fe, Mn, Mg, Zn, and Cu in soft body tissue—the highest percentage deviation was −3.89% for Fe.

The accuracy of prediction shows that the multivariate chemometrics analytical models developed here would be useful in noninvasive cancer diagnostics utilizing biometals as the disease biomarkers because trace bimetals offer the potential for early detection, tracking progression and recurrence, as well as monitoring of treatment response intrinsically in tissue.

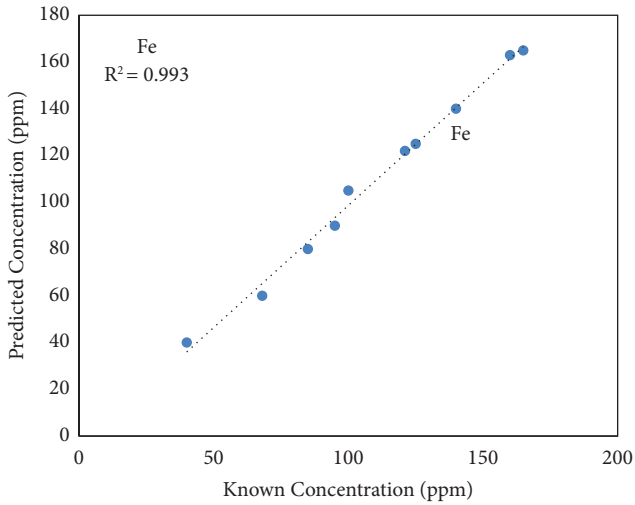

Figure 4: Artificial neural network regression curve of predicted versus known concentration of iron.

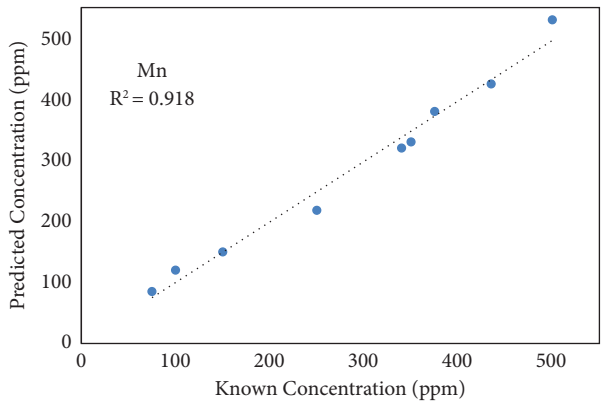

Figure 5: Artificial neural network regression curve of predicted versus known concentration of manganese.

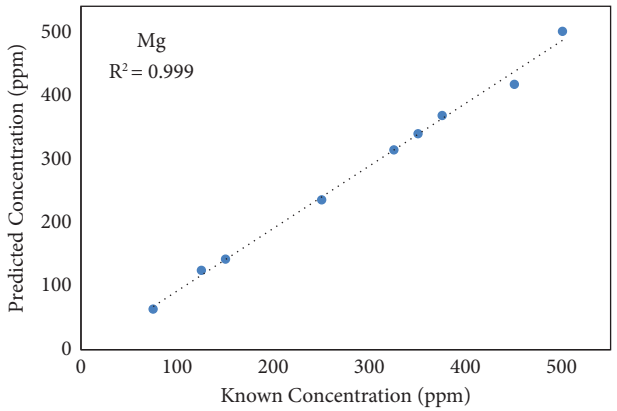

Figure 6: Artificial neural network regression curve of predicted versus known concentration of magnesium.

3. Results and Discussion

3.1. Method Application to Needle Tissue Biopsies. To better understand the metallome in disease, the determination of actual samples is of great importance [28]. The developed

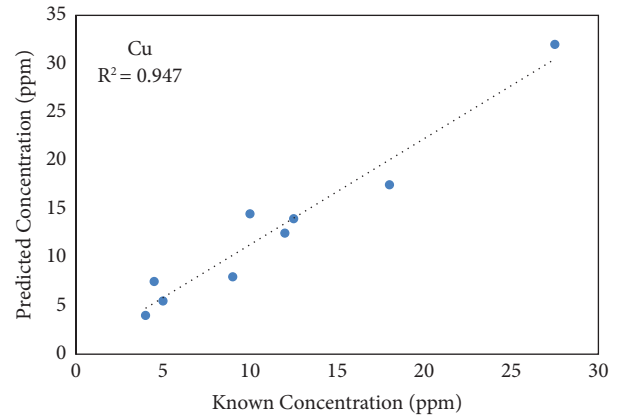

Figure 7: Artificial neural network regression curve of predicted versus known concentration of copper.

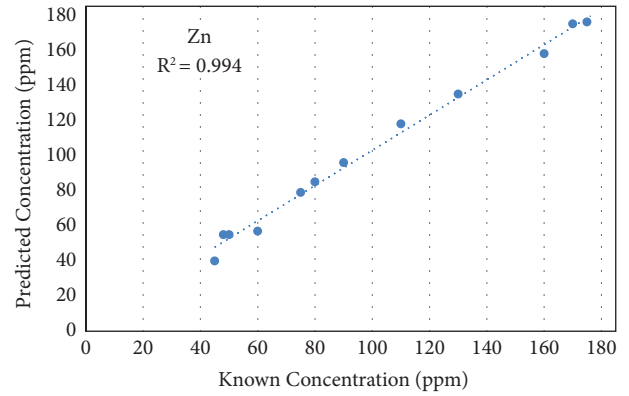

Figure 8: Artificial neural network regression curve of predicted versus known concentration of zinc.

analytical models were investigated preliminarily on the liver, breast, and abdominal needle biopsies described above, and the results are shown in Table 2. The concentration ranges determined for the tissues were Fe (51.2–137.2 μg/g), Cu (5–18.7 μg/g), Zn (36–56.8 μg/g), Mg (78.2–507.4 μg/g), and Mn (8.8–19.5 μg/g) for liver; Fe (87.7–113.9 μg/g), Cu (10.9–12.3 μg/g), Zn (49.3 μg/g–55.7 μg/g), Mg (194.3–242.3 μg/g), and Mn (14.5 μg/g–16.1 μg/g) for breast; and Fe (96.7–125.7 μg/g), Cu (6.7–7.5 μg/g), Zn (88.3–93.9 μg/g), Mg (467.5–583.1 μg/g), and Mn (9.5–10.5 μg/g) for abdominal, respectively.

The biometal concentrations in healthy and diseased (cancer) tissues are clearly different, as previously reported [29, 30]. From Table 2, liver tissue sample number 2 and the abdominal samples, which had been histologically classified as malignant, had higher concentrations of Fe and relatively low concentrations of Cu as compared to the other liver tissue, which had been classified as benign. This shows there is an increased need for Fe in proliferating tissues due to the constant demand for supply of nutrients. The results for malignant and benign liver tissues clearly indicate the presence of cancer based on the trace biometals, which is in agreement with their pathological examination. It was also observed by other workers that the concentrations of Ca, Fe, Cu, and Zn are higher in neoplastic tissues (malignant and

Table 1: Summary of certified versus predicted concentrations of iron, manganese, magnesium, zinc, and copper in oyster tissue (NIST 1566B).

Element	Oyster tissue standard concentration (μg/g)	Predicted concentration (μg/g)	Percent deviation (%)
Fe	205.8 ± 6.8	213 ± 28	−3.89
Mn	18.5 ± 0.2	18.1 ± 0.9	2.16
Mg	1085 ± 23	1068 ± 117	1.57
Cu	71.7 ± 1.6	70.2 ± 4.2	2.15
Zn	1424 ± 46	1418 ± 127	0.42

Table 2: Predicted concentration values of copper, manganese, magnesium, iron, and zinc in liver tissues using the artificial neural network multivariate calibration models.

Tissue	Mg (μg/g)	Mn (μg/g)	Fe (μg/g)	Cu (μg/g)	Zn (μg/g)
Liver 1	87.9 ± 9.7	18.6 ± 0.9	58.9 ± 7.7	17.6 ± 1.1	39.6 ± 3.6
Liver 2	457.1 ± 50.3	9.3 ± 0.5	121.4 ± 15.8	5.3 ± 0.3	52.1 ± 4.7
Abdominal	525.3 ± 57.8	10.0 ± 0.5	111.2 ± 14.5	7.1 ± 0.4	88.6 ± 5.3
Breast	218.3 ± 24.0	15.3 ± 0.8	100.8 ± 13.1	11.6 ± 0.7	52.5 ± 3.2

benign) when compared with normal tissues [31, 32]. These trace biometals can be considered tumour biomarkers because it is possible to classify different tissues as normal or neoplastic, as well as different types of cancer, based on their concentrations. Further, all the trace biometals were statistically correlated with well-known prognostic factors for breast cancer.

4. Conclusion

This work involved the evaluation of a rapid chemometric peak-free LIBS technique for direct rapid (diagnostic) analysis of trace biometals in soft body tissue. A multivariate chemometrics calibration model was developed using ANN and based on paraffin wax for the determination of the concentrations of Fe, Mn, Mg, Cu, and Zn in soft body tissue. The model was successfully validated using oyster tissue as a certified reference material (CRM). The predicted biometal concentrations were within a range of less than 5% error. This work has demonstrated that LIBS can be a useful technique for rapidly and directly detecting trace amounts of biometals in soft body tissue in the context of spectral diagnostics of disease. The method was tested on malignant and benign liver tissues, and the results agreed with those of histopathological examination, which is based on the microscopic examination of tissue morphology. Although the sample numbers in this work were too few to accurately assess the deviation between healthy and diseased tissue based on the analysed biometals, the method is not only potentially accurate but is useful for rapid diagnostics of cancer in soft body tissues. In a typical application, the analysed biomarkers would be measured and monitored to yield specific signatures that can be used for detecting cancer early before morphological features become apparent.

Data Availability

The datasets used in the study are available from the corresponding author upon request.

Conflicts of Interest

The authors declare that they have no conflicts of interest.

Authors' Contributions

OEA prepared the simulated samples, collected spectral data, performed statistical and chemometric analyses of the samples, and prepared the initial draft of the manuscript. AHK and DKA conceived the project. AHK and DKA supervised data collection and chemometric analyses and provided feedback and suggestions on the manuscript before submission. All authors read and agreed with the final version of the manuscript.

Acknowledgments

The authors acknowledge the Swedish International Development Cooperation Agency (SIDA), through the International Science Programme (ISP), Uppsala University, for financial support in the form of a research grant (KEN: 04), which was used to purchase the LIBS spectrometer. The authors also wish to acknowledge the International Science Programme (ISP) of Sweden for awarding an MSc study fellowship to the first author.

References

[1] E. Srivastava, H. Jang, S. Shin, J. Choi, S. Jeong, and E. Hwang, "Weighted-averaging-based classification of laser-induced breakdown spectroscopy measurements using most informative spectral lines," *Plasma Science and Technology*, vol. 22, no. 1, Article ID 015501, 2020.

[2] S. Yao, J. Zhao, J. Xu, Z. Lu, and J. Lu, "Optimizing the binder percentage to reduce matrix effects for the LIBS analysis of carbon in coal," *Journal of Analytical Atomic Spectrometry*, vol. 32, no. 4, pp. 766–772, 2017.

[3] Q. Q. Wang, G. Teng, X. L. Qiao et al., "Importance evaluation of spectral lines in laser-induced breakdown spectroscopy for classification of pathogenic bacteria," *Biomedical Optics Express*, vol. 9, no. 11, pp. 5837–5850, 2018.

[4] J. H. Han, Y. Moon, J. J. Lee, S. Choi, Y. C. Kim, and S. Jeong, "Differentiation of cutaneous melanoma from surrounding skin using laser-induced breakdown spectroscopy," *Biomedical Optics Express*, vol. 7, no. 1, pp. 57–66, 2016.

[5] G. Teng, Q. Wang, H. Zhang et al., "Discrimination of infiltrative glioma boundary based on laser-induced breakdown spectroscopy," *Spectrochimica Acta Part B: Atomic Spectroscopy*, vol. 165, Article ID 105787, 2020.

[6] C. G. Fraga, "Relevance, essentiality and toxicity of trace elements in human health," *Molecular Aspects of Medicine*, vol. 26, no. 4-5, pp. 235–244, 2005.

[7] A. Miziolek, V. Palleschi, and I. Schecter, *Laser-Induced Breakdown Spectroscopy (LIBS) Fundamentals and Applications*, Cambridge University Press, Cambridge, UK, 2006.

[8] J. P. Singh and S. N. Thakur, *Laser-induced Breakdown Spectroscopy*, Elsevier, Amsterdam, 2007.

[9] L. J. Radziemski and D. A. Cremers, *Laser-Induced Plasma and Applications*, Marcel Dekker, New York, NY, USA, 1989.

[10] R. Noll, *Laser-Induced Breakdown Spectroscopy: Fundamentals and Applications*, Springer, Heidelberg, Germany, 2012.

[11] E. Tognoni, V. Palleschi, M. Corsi, and G. Cristoforetti, "Quantitative micro-analysis by laser-induced breakdown spectroscopy - a review of the experimental approaches," *Spectrochimica Acta Part B: Atomic Spectroscopy*, vol. 57, no. 7, pp. 1115–1130, 2002.

[12] D. Santos Jr., R. E. Samad, L. C. Trevizan, A. Z. de Freitas, N. D. Vieira Jr., and F. J. Krug, "Evaluation of femtosecond laser-induced breakdown spectroscopy for analysis of animal tissues," *Applied Spectroscopy*, vol. 62, no. 10, pp. 1137–1143, 2008.

[13] M. D. Adamson and S. J. Rehse, "Detection of trace Al in model biological tissue with laser-induced breakdown spectroscopy," *Applied Optics*, vol. 46, no. 23, pp. 5844–5852, 2007.

[14] A. Ciucci, M. Corsi, V. Palleschi, S. Rastelli, A. Salvetti, and E. Tognoni, "New procedure for quantitative elemental analysis by laser-induced plasma spectroscopy," *Applied Spectroscopy*, vol. 53, no. 8, pp. 960–964, 1999.

[15] T. Zhang, H. Tang, and H. Li, "Chemometrics in laser-induced breakdown spectroscopy," *Journal of Chemometrics*, vol. 32, no. 11, p. e2983, 2018.

[16] D. F. Andrade and E. R. Pereira Filho, "Direct determination of contaminants and major and minor nutrients in solid fertilizers using laser-induced breakdown spectroscopy (LIBS)," *Journal of Agricultural and Food Chemistry*, vol. 64, no. 41, pp. 7890–7898, 2016.

[17] T. Zhang, L. Liang, K. Wang et al., "A novel approach for the quantitative analysis of multiple elements in steel based on laser-induced breakdown spectroscopy (LIBS) and random forest regression (RFR)," *Journal of Analytical Atomic Spectrometry*, vol. 29, no. 12, pp. 2323–2329, 2014.

[18] S. A. Kalogirou, "Applications of artificial neural-networks for energy systems," *Applied Energy*, vol. 67, no. 1-2, pp. 17–35, 2000.

[19] P. Mukhono, "Chemometrics-assisted laser induced breakdown spectroscopy of high background radiation area geothermal field matrices," MSc Thesis, University of Nairobi, Nairobi, Kenya, 2012.

[20] E. F. Petricoin, A. M. Ardekani, B. A. Hitt et al., "Use of proteomic patterns in serum to identify ovarian cancer," *The Lancet*, vol. 359, no. 9306, pp. 572–577, 2002.

[21] G. Mor, I. Visintin, Y. Lai et al., "Serum protein markers for early detection of ovarian cancer," *Proceedings of the National Academy of Sciences*, vol. 102, no. 21, pp. 7677–7682, 2005.

[22] J. Versieck and R. Cornelis, *Trace Elements in Human Plasma or Serum*, CRC Press, Boca Raton, FL, USA, 1989.

[23] A. Quentmeier, W. Sdorra, and K. Niemax, "Internal standardization in laser induced fluorescence spectrometry of microplasmas produced by laser ablation of solid samples," *Spectrochimica Acta Part B: Atomic Spectroscopy*, vol. 45, no. 6, pp. 537–546, 1990.

[24] L. N. Li, X. F. Liu, F. Yang, W. M. Xu, J. Y. Wang, and R. Shu, "A review of artificial neural network based chemometrics applied in laser-induced breakdown spectroscopy analysis," *Spectrochimica Acta Part B: Atomic Spectroscopy*, vol. 180, Article ID 106183, 2021.

[25] F. Marini, R. Bucci, A. L. Magrì, and A. D. Magrì, "Artificial neural networks in Chemometrics: History, Examples and Perspectives," *Microchemical Journal*, vol. 88, no. 2, 2008.

[26] M. Khayatzadeh Mahani, M. Chaloosi, M. Ghanadi Maragheh, A. R. Khanchi, and D. Afzali, "Comparison of artificial neural networks with partial least squares regression for simultaneous determinations by ICP-AES," *Chinese Journal of Chemistry*, vol. 25, no. 11, pp. 1658–1662, 2007.

[27] S. D. Kamath, C. S. D'souza, S. Mathew, S. D. George, C. Santhosh, and K. K. Mahato, "A pilot study on colonic mucosal tissues by fluorescence spectroscopy technique: discrimination by principal component analysis (PCA) and artificial neural network (ANN) analysis," *Journal of Chemometrics*, vol. 22, no. 6, pp. 408–416, 2008.

[28] R. Zhang, L. Li, Y. Sultanbawa, and Z. P. Xu, "X-ray fluorescence imaging of metals and metalloids in biological systems," *American Journal of Nuclear Medicine and Molecular Imaging*, vol. 8, no. 3, pp. 169–188, 2018.

[29] O. Samek, H. H. Telle, and D. C. Beddows, "Laser-induced breakdown spectroscopy: a tool for real-time, in vitro and in vivo identification of carious teeth," *BMC Oral Health*, vol. 1, pp. 1–9, 2001.

[30] M. Corsi, G. Cristoforetti, M. Hidalgo et al., "Application of laser-induced breakdown spectroscopy technique to hair tissue mineral analysis," *Applied Optics*, vol. 42, no. 30, pp. 6133–6137, 2003.

[31] J. Wang, L. Li, P. Yang et al., "Identification of cervical cancer using laser-induced breakdown spectroscopy coupled with principal component analysis and support vector machine," *Lasers in Medical Science*, vol. 33, no. 6, pp. 1381–1386, 2018.

[32] M. P. Silva, D. F. Soave, A. Ribeiro-Silva, and M. E. Poletti, "Trace elements as tumor biomarkers and prognostic factors in breast cancer: a study through energy dispersive x-ray fluorescence," *BMC Research Notes*, vol. 5, no. 1, p. 194, 2012.